Received: 22 February 2020 | Revised: 11 July 2020 | Accepted: 19 August 2020

DOI: 10.1002/bit.27544

ARTICLE

BIOTECHNOLOGY AND BIOENGINEERING WILEY

Kinetic modeling of microbial growth, enzyme activity, and gene deletions: An integrated model of β-glucosidase function in *Cellvibrio japonicus*

Jeanice Hwang | Archana Hari | Raymond Cheng | Jeffrey G. Gardner | Daniel Lobo

Department of Biological Sciences, University of Maryland, Baltimore County, Baltimore, Maryland, USA

Correspondence
Daniel Lobo, Department of Biological Sciences, University of Maryland, Baltimore County, 1000 Hilltop Circle, Baltimore, MD 21250, USA.
Email: lobo@umbc.edu

Funding information
National Science Foundation, Grant/Award Number: OAC-1726023; U.S. Department of Energy, Grant/Award Number: DE-SC0014183

Abstract

Understanding the complex growth and metabolic dynamics in microorganisms requires advanced kinetic models containing both metabolic reactions and enzymatic regulation to predict phenotypic behaviors under different conditions and perturbations. Most current kinetic models lack gene expression dynamics and are separately calibrated to distinct media, which consequently makes them unable to account for genetic perturbations or multiple substrates. This challenge limits our ability to gain a comprehensive understanding of microbial processes towards advanced metabolic optimizations that are desired for many biotechnology applications. Here, we present an integrated computational and experimental approach for the development and optimization of mechanistic kinetic models for microbial growth and metabolic and enzymatic dynamics. Our approach integrates growth dynamics, gene expression, protein secretion, and gene-deletion phenotypes. We applied this methodology to build a dynamic model of the growth kinetics in batch culture of the bacterium *Cellvibrio japonicus* grown using either cellobiose or glucose media. The model parameters were inferred from an experimental data set using an evolutionary computation method. The resulting model was able to explain the growth dynamics of *C. japonicus* using either cellobiose or glucose media and was also able to accurately predict the metabolite concentrations in the wild-type strain as well as in β-glucosidase gene deletion mutant strains. We validated the model by correctly predicting the non-diauxic growth and metabolite consumptions of the wild-type strain in a mixed medium containing both cellobiose and glucose, made further predictions of mutant strains growth phenotypes when using cellobiose and glucose media, and demonstrated the utility of the model for designing industrially-useful strains. Importantly, the model is able to explain the role of the different β-glucosidases and their behavior under genetic perturbations. This integrated approach can be extended to other metabolic pathways to produce mechanistic models for the comprehensive understanding of enzymatic functions in multiple substrates.

KEYWORDS
cellobiose, *Cellvibrio japonicus*, kinetic modeling, kinetic parameter estimation, β-glucosidase

1 | INTRODUCTION

Gaining a mechanistic understanding of microbial metabolic processes including their dynamic and regulatory aspects will be essential to address many biological and industrial problems (Millard, Smallbone, & Mendes, 2017). Experimental approaches such as genetic knockouts of key enzymes can be used to analyze the resultant growth dynamics and determine the physiological functions of each component of a metabolic pathway (Wu, Du, Chen, & Zhou, 2015). Furthermore, extracting mechanistic knowledge from these datasets towards quantitative predictions in terms of growth dynamics under different conditions requires system-level kinetic modeling able to account for the degradation of multiple metabolites by different enzymes and under various growth conditions (Kurata & Sugimoto, 2018; Steuer, Gross, Selbig, & Blasius, 2006). However, traditional kinetic models lack genetic and enzymatic dynamics and are usually calibrated for predicting growth using only a single substrate (Park, Lang, Thamaraiselvi, Kukor, & Abriola, 2008). Consequently, more sophisticated kinetic models are needed for gaining a comprehensive understanding of specific microbial degradation pathways that can predict multiple enzyme functions and growth dynamics under complex substrate conditions and genetic perturbations (Smallbone et al., 2013).

Polysaccharides are the most abundant carbon compounds in the biosphere, and have numerous applications in the biomedical, chemical, and renewable energy industries (Jeoh, Cardona, Karuna, Mudinoor, & Nill, 2017). However, recovering the nutrients locked away in insoluble polysaccharides, such as lignocellulose, is a major challenge for environmental bacteria due to the complexities of the substrate (Kuusk, Sørlie, & Väljamäe, 2015). Some environmental microbes are able to degrade insoluble polysaccharides by expressing carbohydrate active enzymes (CAZymes; Nelson, Attia, et al., 2017). For example, *Cellvibrio japonicus* is a model bacterium able to completely degrade all of the major plant cell wall polysaccharides (DeBoy et al., 2008). This bacterium possesses at least twelve endoglucanases, one cellobiohydrolase, and four β-glucosidases, and previous genetic and biochemical studies have shown the importance of these CAZymes for *C. japonicus* to degrade and metabolize both pure cellulose as well as corn stover (Gardner & Keating, 2010; Gardner et al., 2014; Nelson & Gardner, 2015). A more recent report described in detail the later stages of cellulose degradation by *C. japonicus*, and discussed the nonredundant functions of four β-glucosidases participating in the degradation of cellodextrins (Nelson, Rogowski, et al., 2017). While obtaining a mechanistic understanding of the in vivo physiological roles of cellulose-degrading CAZymes required genetic and biochemical data, what is now needed are methods to use those data to further predict the growth dynamics of bacteria under multiple substrates and after deletion of specific genes. Furthermore, any generated models need to be constructed with an emphasis on the discovery and manipulation of the most relevant metabolic pathways.

A number of kinetic models have been proposed for describing microbial growth on cellulosic substrates, but they are based on traditional Michaelis–Menten for enzymatic reactions and Monod for microbial growth without considering multiple substrates or bacterial strains possessing genetic perturbations. For example, the saccharification or fermentation of cellulose by bacteria or yeast together with their growth in both batch and continuous cultures have been empirically modeled with kinetic models based on Langmuir absorption equations for cellulose degradation, Michaelis–Menten kinetics for β-glucosidase reactions, and Monod models for cell biomass growth. These approaches make use of yield coefficients to directly link substrate concentrations to cell biomass growth, either with a single yield coefficient from glucose (Mutturi & Lidén, 2014; Oh, Kim, Jeong, & Hong, 2000; Philippidis & Hatzis, 1997; Sakimoto, Kanna, & Matsumura, 2017) or with separated experiment-specific coefficients to explain the growth dynamics on different substrates (Fox, Levine, Blanch, & Clark, 2012; Gomez-Flores, Nakhla, & Hafez, 2015, 2017; Kwon & Engler, 2005; Moldes, Alonso, & Parajó, 1999). In addition, models explicitly including the function of enzymes have been proposed for the enzymatic saccharification of lignocellulose. However, these approaches either omit cell biomass growth (Kadam, Rydholm, & McMillan, 2004), lump all enzyme concentrations together (Shen & Agblevor, 2010), or include different coefficients for different substrates (Shin, Yoo, Kim, & Yang, 2006), preventing the understanding of specific enzyme functions or with multiple substrates. Constant enzyme concentrations have been also used to predict different dynamics during the saccharification and fermentation of cellulose to ethanol and cell biomass (Shadbahr, Khan, & Zhang, 2017). Overall, current modeling approaches for cellodextrins degradation and microbial growth lack the ability to model the physiological function of individual enzymes when a bacterium is metabolizing different substrates. New modeling approaches are needed to obtain a better understanding of the dynamic roles of the enzymes participating in cellulose degradation (Steuer et al., 2006).

Here we present a combined in vivo and in silico approach for developing a kinetic metabolic model of cellobiose degradation in *Cellvibrio japonicus*. Our modeling strategy is able to recapitulate the dynamics of cell growth and metabolite consumption while accounting for different genetic perturbations and growth with multiple substrates. The model integrates data for the expression of β-glucosidase genes participating in extra- and intracellular metabolic reactions. A computational optimization methodology was developed to infer the parameters of the model from data collected using both wild-type and mutant strains of *C. japonicus* and could accurately recapitulate the growth dynamics of all strains. The model was then validated by the prediction of growth dynamics in a mixed medium with cellobiose and glucose, which was predicted to be co-utilized and subsequently observed in vivo. Finally, we made predictions of the growth dynamics of the mutant strains during co-utilization of both cellobiose and glucose and designed strain optimization strategies for the maximization of the specific degradation rate of cellobiose in *C. japonicus*. In summary, the presented approach can provide a detailed mechanistic understanding of the metabolic pathways essential in cellulose degradation and will aid in advanced metabolic engineering optimizations.

2 | MATERIALS AND METHODS

2.1 | Growth and metabolic analyses

The *C. japonicus* strains used in this study were the wild-type strain (Ueda107), and three β-glucosidase mutants derived from wild-type (Δ*cel3A*, Δ*cel3B*, and Δ*cel3A* Δ*cel3B*). The construction of the mutant strains has been described previously (Nelson, Attia, et al., 2017; Nelson, Rogowski, et al., 2017). Single colonies of these strains were used to inoculate three 18-mm test tubes each containing 5 ml of 3-(*N*-morpholino)propanesulfonic acid (MOPS) defined medium with glucose (0.2% wt/vol) as the sole carbon source. These inocula were incubated for 24 h at 30°C with a high level of aeration (200 RPM) and then used to inoculate Erlenmeyer flasks that contained 500 ml MOPS defined medium. The flasks were inoculated with a dilution ratio of 1:100. The flasks contained MOPS defined media with glucose (0.25% wt/vol), cellobiose (0.25% wt/vol), or a mixture of cellobiose and glucose (0.125% wt/vol for each carbon source). Three flasks of each carbon source were used for the growth and metabolite experiments. After inoculation in the flasks, a 10 ml sample was collected every hour for 24 h and cell density was measured as absorbance at 600 nm using a Spec20D+ spectrophotometer (Thermo Fisher Scientific), which was then interpolated to dry weight using an experimentally determined linear conversion factor of $[gL^{-1}] = 0.8994 \cdot [OD_{600}]$. From the 10 ml sample, three 500 μl aliquots were dispensed in 1.5 ml microcentrifuge tubes and spun at 21130 RCF on a tabletop centrifuge (Eppendorf). The pellets were discarded and the supernatants were filtered through 0.2 μm nylon syringe cartridges (Thermo Fisher Scientific). The concentration of glucose and cellobiose that remained in the supernatants was determined by HPAEC-PAD as done previously (Nelson, Rogowski, et al., 2017). Briefly, we used a Dionex ICS-5000$^+$ system (Thermo Fisher Scientific) equipped with a 4 × 250 mm SA-10 anion-exchange column and a 4 × 50 mm SA-10 guard column. A sample volume of 25 μl was injected into an isocratic gradient with a flow rate of one mL/min of 20 mM sodium hydroxide with the column temperature set to 30°C. To ensure data robustness, all in vitro experiments were performed in both technical and biological triplicate. Preliminary data analysis used the Dionex Chromeleon 7 and GraphPad Prism 6 software packages.

2.2 | Model simulation and parameter estimation

We developed a simulator for kinetic models including metabolites, enzymes, and microbial growth represented by a system of ordinary differential equations (ODEs), together with an optimization methodology based on genetic algorithms to infer the kinetic parameters directly from experimental data (Lobikin et al., 2015; Lobo & Levin, 2015; Lobo & Vico, 2010a, 2010b). Models are numerically solved with LSODA (Petzold, 1983); mutant strains with gene knockouts are simulated by keeping the concentration and rate of the eliminated enzymes as zero. Enzymatic parameters of known enzymes are based on experimental values (Nelson, Rogowski, et al., 2017), whereas the rest were inferred with the optimization methodology. In brief, the genetic algorithm evolves a population of individuals, each representing a set of parameters in the model. For each generation, the individuals in the population are selected, crossed, mutated, simulated and their fitness scored. This iterative process runs until no better model is found for 1000 generations. To improve performance and preserve genetic diversity, the population follows an island distribution approach (Whitley, Rana, & Heckendorn, 1999) with 32 parallel subpopulations with 64 individuals each; every 1000 generations the islands are randomly paired and their individuals shuffled. Cross-over produces new individuals by randomly combining two existing ones, mutations randomly change the parameters of an individual, each with 1% probability, following a uniform distribution, and selection chooses the next population among the current and new individuals using a deterministic crowding method (Mahfoud, 1992). Quotients involved in enzyme production (h^{-1}) have a range of (0, 10^9); quotients representing catalyst constant (h^{-1}) or maximum velocity ($g\,L^{-1}\,h^{-1}$) degradation rates, uptake rates ($g\,L^{-1}\,h^{-1}$), and saturation and inhibition constants ($g\,L^{-1}$) have a range of (0, 10^6); specific coefficients of expression rates (dimensionless), specific rate of cell biomass to glucose ($g\,L^{-1}$), and decay rate (h^{-1}) have a range of (0, 1). The initial population consists of individuals with uniform random parameters within their range. The fitness of an individual represents its ability to recapitulate the training data set of microbial growth experiments, calculated as the normalized root mean square error averaged among all the curves and experiments in the data set with

$$\frac{1}{M}\sum_{i=1}^{M}\frac{1}{N_i}\sum_{j=1}^{N_i}\frac{\sqrt{\frac{1}{P_{i,j}}\sum_{k=1}^{P_{i,j}}(y_{i,j,k}-\hat{y}_{i,j,k})^2}}{\hat{y}_{i,j,\max}-\hat{y}_{i,j,\min}}, \quad (1)$$

where M is the number of training experiments, N_i is the number of experimental curves (either metabolites or cell biomass concentrations) in experiment i, $P_{i,j}$ is the number of data points in curve j in experiment i, and $y_{i,j,k}$, $\hat{y}_{i,j,k}$, $\hat{y}_{i,j,\max}$, and $\hat{y}_{i,j,\min}$ are the predicted, experimental, maximum, and minimum data point k, of curve j, in experiment i, respectively. The simulation, optimization, visualization, and statistical algorithms were implemented in C++ using the Standard, Eigen (http://eigen.tuxfamily.org), Qt (The Qt Company Ltd.), and Qwt (Uwe Rathmann and Josef Wilgen) libraries.

2.3 | Data analysis

The coefficient of determination (R^2) was implemented between the experimental data and the model's predictions to evaluate its precision. A value closer to 1 indicates a higher correlation and that the resulting model simulation can accurately describe the experimental data. Growth rates of in vivo experiments averages and in silico simulations were computed as in (Hall, Acar, Nandipati, & Barlow, 2014) with a 3-h window. Cellobiose-specific degradation rates were calculated in the midpoint of the exponential phase as determined in the growth rate computation.

3 | RESULTS

3.1 | Mathematical model of microbial growth and enzymatic activity

We developed a kinetic model of *C. japonicus* growth in batch culture including enzyme expression and substrate uptake, degradation, and conversion to cell biomass. The model includes the metabolites glucose and cellobiose (both intra- and extracellular), β-glucosidase enzymes (including intracellular Cel3A and Cel3B (Nelson, Rogowski, et al., 2017) and other β-glucosidases lumped together as either intra- or extracellular enzymes), and cell biomass concentration. Figure 1 shows a diagram of the cell with the components and reactions included in the model.

When degraded extracellularly, cellobiose is converted to glucose by secreted β-glucosidases following Michaelis–Menten kinetics such that

$$v_{cge} = \frac{\beta_{cge} \cdot e_e \cdot c_e}{K_{cge} + c_e}, \tag{2}$$

where ν_{cge} is the velocity of the extracellular conversion of cellobiose into glucose, c_e is the concentration of extracellular cellobiose, e_e is the concentration of extracellular β-glucosidases lumped together, β_{cge} is the specific rate, and K_{cge} is the saturation constant.

Similarly, intracellular cellobiose is degraded to glucose by intracellular β-glucosidases, including Cel3A, Cel3B, and others lumped together following Michaelis–Menten kinetics, resulting in

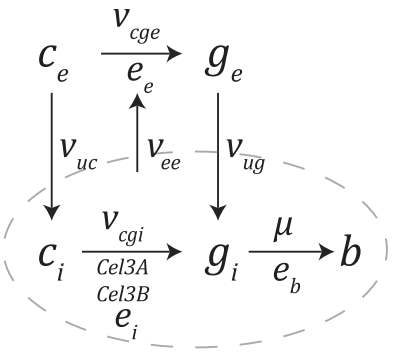

FIGURE 1 Diagram of the proposed model for *Cellvibrio japonicus* growth, β-glucosidases expression and activity, and uptake and degradation of cellobiose and glucose. Extracellular cellobiose (c_e) is either degraded at rate v_{cge} to extracellular glucose (g_e) by β-glucosidase enzymes lumped together (e_e) secreted at rate v_{ee} or uptaken into the cell at rate v_{uc} as intracellular cellobiose (c_i). Extracellular glucose is uptaken into the cell as intracellular glucose (g_i) at rate v_{ug}. Intracellular cellobiose is degraded to intracellular glucose by Cel3A, Cel3B, and other lumped intracellular β-glucosidases (e_i) at rate v_{cgi}. Intracellular glucose is then converted into cell biomass (b) at specific growth rate μ by a reaction involving multiple enzymes lumped together (e_b). Dashed oval represents the bacterial cell

$$v_{cgi} = v_{cgCel3A} + v_{cgCel3B} + v_{cgo},$$

$$v_{cgCel3A} = \frac{\beta_{cgiCel3A} \cdot Cel3A \cdot c_i}{K_{cgiCel3A} + c_i},$$

$$v_{cgCel3B} = \frac{\beta_{cgiCel3B} \cdot Cel3B \cdot c_i}{K_{cgiCel3B} + c_i},$$

$$v_{cgo} = \frac{\beta_{cgo} \cdot e_i \cdot c_i}{K_{cgo} + c_i}, \tag{3}$$

where v_{cgi} is the combined reaction velocity and $v_{cgCel3A}$, $v_{cgCel3B}$, and v_{cgo} are the reaction velocities for each particular enzymatic reaction, Cel3A, Cel3B, and $e_i$are the intracellular concentration of Cel3A, Cel3B, and other β-glucosidases lumped together, respectively, $c_i$is the concentration of intracellular cellobiose, $\beta_{cgiCel3A}$, $\beta_{cgiCel3B}$, and β_{cgo} are the specific rates, and $K_{cgiCel3A}$, $K_{cgiCel3B}$, and K_{cgo} the saturation constants.

Uptake kinetics are modeled with facilitated diffusion, since genomic analyses of *C. japonicus* have shown a lack of phosphotransferase systems (PTS) for utilization of cellobiose or glucose, as it is the case in the pseudomonads family (Rojo, 2010) and other obligate aerobes (Riemann & Azam, 2002). In this way, both extracellular cellobiose and extracellular glucose are uptaken by the cell with an inhibition term to model the kinetics of facilitated diffusion, resulting in

$$v_{uc} = \frac{\beta_{uc} \cdot c_e}{K_{uc}\left(1 + \frac{c_i}{K_{ic}}\right) + c_e},$$

$$v_{ug} = \frac{\beta_{ug} \cdot g_e}{K_{ug}\left(1 + \frac{g_i}{K_{ig}}\right) + g_e}, \tag{4}$$

where v_{uc} and v_{ug} are the uptake rates of cellobiose and glucose, respectively, g_e and g_i are the concentrations of extracellular and intracellular glucose, respectively, β_{uc} and β_{ug} are the maximum rates, K_{uc} and K_{ug} are the saturation constants, and K_{ic} and K_{ig} are the inhibition constants.

Intracellular glucose is degraded into cell biomass precursors, which is modeled as a lumped reaction based on Michaelis–Menten kinetics such that

$$v_{gb} = \frac{\beta_{gb} \cdot e_b \cdot g_i}{K_{gb} + g_i}, \tag{5}$$

where v_{gb} is the degradation velocity, e_b are the lumped enzymes, β_{gb} is the specific rate, and K_{gb} is the saturation constant.

The specific microbial growth rate μ depends on the degradation velocity of intracellular glucose, resulting in

$$\mu = K_u \cdot v_{gb}, \tag{6}$$

where K_u is a lumped conversion constant from glucose to biomass, an approach previously used to model the specific microbial growth

rate from production rates of intracellular metabolites (Jahan, Maeda, Matsuoka, Sugimoto, & Kurata, 2016; Kadir, Mannan, Kierzek, McFadden, & Shimizu, 2010; Kurata & Sugimoto, 2018).

The rate of cell biomass concentration includes also a decay term, resulting in

$$\frac{db}{dt} = \mu \cdot b - K_d \cdot b, \tag{7}$$

where b is the concentration of cell biomass and K_d is the decay constant.

Enzymes are expressed depending on the intracellular concentration of their respective substrates and modulated by the concentration of intracellular glucose, which acts as a proxy for the available energy in the cell such that

$$v_{eb} = \frac{\beta_{eb} \cdot g_i}{K_{eb} + g_i},$$

$$v_{Cel3A} = \frac{\beta_{Cel3A} \cdot c_i \cdot g_i}{K_{Cel3A} + c_i},$$

$$v_{Cel3B} = \frac{\beta_{Cel3B} \cdot c_i \cdot g_i}{K_{Cel3B} + c_i},$$

$$v_{ei} = \frac{\beta_{ei} \cdot c_i \cdot g_i}{K_{ei} + c_i},$$

$$v_{ee} = \frac{\beta_{ee} \cdot c_i \cdot g_i}{K_{ee} + c_i}, \tag{8}$$

where v_{eb}, v_{Cel3A}, v_{Cel3B}, v_{ei}, v_{ee} are the velocities of expression of the lumped biomass precursor enzymes, Cel3A, Cel3B, other internal β-glucosidases, and the secreted β-glucosidases, respectively, β_{eb}, β_{Cel3A}, β_{Cel3B}, β_{ei}, and β_{ee} are the specific rates, and K_{ei}, K_{Cel3A}, K_{Cel3B}, K_{ei}, and K_{ee} are the saturation constants.

The intracellular enzymatic concentrations are diluted due to the collective cell volume increase during microbial growth, resulting in

$$\frac{de_i}{dt} = K_{gei} \cdot v_{ei} - \mu \cdot e_i,$$

$$\frac{de_b}{dt} = K_{geb} \cdot v_{eb} - \mu \cdot e_b,$$

$$\frac{dCel3A}{dt} = K_{gCel3A} \cdot v_{Cel3A} - \mu \cdot Cel3A,$$

$$\frac{dCel3B}{dt} = K_{gCel3B} \cdot v_{Cel3B} - \mu \cdot Cel3B, \tag{9}$$

where K_{gei}, K_{geb}, K_{gCel3A}, and K_{gCel3B} are the specific coefficients of the expression rates. The model omits enzyme degradation terms as a simplification due to the long half-life of bacterial β-glucosidases (Goswami, Gupta, & Datta, 2016; Mehmood, Shahid, Hussain, Latif, & Rajoka, 2014; Meng, Ying, Zhang, Lu, & Li, 2015) compared to the short duration (24 h) of the growth experiments.

Extracellular and intracellular rates of uptaken metabolites and secreted enzymes are converted with a factor of ρ grams of dry cell weight/L of cell volume, estimated to be 564 $g_{DCW}\,L^{-1}$ as used before (Chassagnole, Noisommit-Rizzi, Schmid, Mauch, & Reuss, 2002; Jahan et al., 2016; Kurata & Sugimoto, 2018), such that

$$v_{ug,medium} = v_{ug} \cdot \frac{b}{\rho},$$

$$v_{uc,medium} = v_{uc} \cdot \frac{b}{\rho},$$

$$v_{ee,medium} = v_{ee} \cdot \frac{b}{\rho}, \tag{10}$$

where $v_{ug,medium}$ and $v_{uc,medium}$ are the uptake rates in media concentration of glucose and cellobiose, respectively, and $v_{ee,medium}$ is the secretion rate in media concentration of lumped extracellular β-glucosidases.

The rate of extracellular enzymatic concentration of lumped extracellular β-glucosidases is hence

$$\frac{de_e}{dt} = K_{gee} \cdot v_{ee,medium}, \tag{11}$$

where K_{gee} is the specific coefficient of expression rate.

The mass balance equations for external and internal cellobiose are hence given by

$$\frac{dc_e}{dt} = -v_{uc,medium} - v_{cge},$$

$$\frac{dc_i}{dt} = v_{uc} - v_{cgi} - \mu \cdot c_i. \tag{12}$$

And the mass balance equation for external glucose takes the form

$$\frac{dg_e}{dt} = 1.053 \cdot v_{cge} - v_{ug,medium}. \tag{13}$$

The mass balance equation for internal glucose also includes depletion terms to account for the production of enzymes, resulting in

$$\frac{dg_i}{dt} = 1.053 \cdot v_{cgi} + v_{ug},$$

$$-v_{gb} - v_{ee} - v_{ei} - v_{eb} - v_{Cel3A} - v_{Cel3B} - \mu \cdot g_i. \tag{14}$$

3.2 | Parameter estimation results

The enzymatic parameters of Cel3A and Cel3B were obtained experimentally (Nelson, Rogowski, et al., 2017) and the rest of the parameters in the model were inferred computationally. We developed an inference methodology based on genetic algorithms—an heuristic optimization approach popular for the optimization of

metabolic models (López-Pérez, Puebla, Velázquez Sánchez, & Aguilar-López, 2016; Neto, Dos Reis Garcia, Rueda, & Da Costa, 2013; Shadbahr, Zhang, Khan, & Hawboldt, 2018)—and a dynamic simulator of metabolic models including multiple substrates and gene deletions. We employed this algorithm to infer a single set of parameters that could recapitulate the microbial growth and metabolite changes from a series of batch cultures that used different carbon sources for both wild-type and mutant strains. The training data set consisted of growth experiments from wild-type *C. japonicus* and β-glucosidase gene deletion strains grown in media containing either glucose or cellobiose as the sole carbon source. The algorithm evolves in silico a population of models (set of real-valued parameters) in an iterative process, where the best models are kept in the population and produces new models by mixing and mutating existent ones. Each new model is simulated with the experimental conditions of the training data set, which includes the measured values of cell biomass and extracellular metabolite concentrations. The remaining variables are initialized with a zero concentration except for intracellular glucose, which starts at a conservative concentration of 0.01 g L^{-1}. After a model is simulated, its growth and metabolic dynamics are compared and scored with respect to the in vivo experiments as the normalized root mean square error. The algorithm stops after no improvement has been found for 1000 generations, and the model with the lowest error is returned.

To test the reproducibility of the inference algorithm, five independent evolutions were run, which took an average of 31 h each

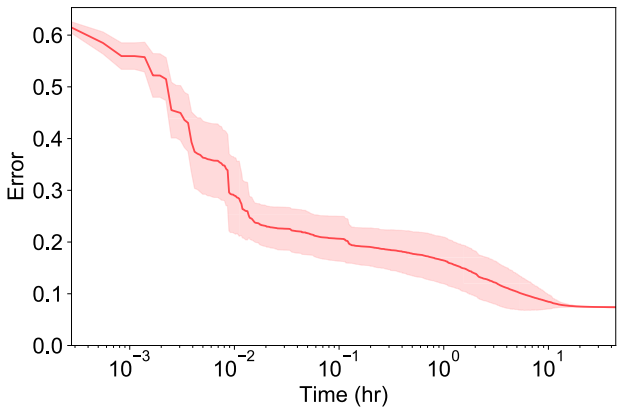

FIGURE 2 Evolutionary optimization runs to infer the model parameters from experimental data. A dynamic simulator and genetic algorithm were implemented to infer unknown model parameters from a training data set containing the growth and metabolic consumption dynamics for wild-type and β-glucosidase gene deletion strains. The graph shows the average normalized root mean square error of the best individual in the population among five independent evolutionary runs. The best-optimized set of parameters among the five evolutions (error of 0.072) was used for the reported model. The shaded area represents standard deviation [Color figure can be viewed at wileyonlinelibrary.com]

TABLE 1 Parameter values of the model, all computationally inferred except the enzymatic parameters of β-glucosidases Cel3A ($\beta_{cgiCel3A}$, $K_{cgiCel3A}$) and Cel3B ($\beta_{cgiCel3B}$, $K_{cgiCel3B}$) that were inferred in vitro (Nelson, Rogowski, et al., 2017), and the specific weight of biomass ρ from Chassagnole et al. (2002)

Parameter	Equation	Value
β_{cge}	(2)	5.04×10^{5} h^{-1}
K_{cge}	(2)	3.29×10^{5} g L^{-1}
$\beta_{cgiCel3A}$	(3)	7.02×10^{3} h^{-1}
$K_{cgiCel3A}$	(3)	0.62 g L^{-1}
$\beta_{cgiCel3B}$	(3)	3.23×10^{5} h^{-1}
$K_{cgiCel3B}$	(3)	0.51 g L^{-1}
β_{cgo}	(3)	7.04×10^{5} h^{-1}
K_{cgo}	(3)	1.93×10^{4} g L^{-1}
β_{uc}	(4)	5.77×10^{5} g L^{-1} h^{-1}
K_{uc}	(4)	2.63×10^{3} g L^{-1}
K_{ic}	(4)	7.57 g L^{-1}
β_{ug}	(4)	1.00×10^{6} g L^{-1} h^{-1}
K_{ug}	(4)	5.08×10^{3} g L^{-1}
K_{ig}	(4)	5.97×10^{5} g L^{-1}
β_{gb}	(5)	5.73×10^{5} h^{-1}
K_{gb}	(5)	1.13×10^{5} g L^{-1}
K_{u}	(6)	1.13×10^{-2} g^{-1} L
K_{d}	(7)	3.84×10^{-3} h^{-1}
β_{eb}	(8)	9.95×10^{8} g L^{-1} h^{-1}
K_{eb}	(8)	3.08×10^{5} g L^{-1}
β_{Cel3A}	(8)	7.19×10^{8} h^{-1}
K_{Cel3A}	(8)	3.96×10^{4} g L^{-1}
β_{Cel3B}	(8)	1.00×10^{9} h^{-1}
K_{Cel3B}	(8)	1.58×10^{4} g L^{-1}
β_{ei}	(8)	1.00×10^{9} h^{-1}
K_{ei}	(8)	7.53×10^{4} g L^{-1}
β_{ee}	(8)	9.97×10^{8} h^{-1}
K_{ee}	(8)	1.55×10^{5} g L^{-1}
K_{gei}	(9)	6.88×10^{-2}
K_{geb}	(9)	8.66×10^{-2}
K_{gCel3A}	(9)	6.49×10^{-3}
K_{gCel3B}	(9)	8.62×10^{-4}
ρ	(10)	564 g_{DCW} L^{-1}
K_{gee}	(11)	0.59

in a single computer node using 36 threads. Figure 2 shows the average evolutionary dynamics of the five independent optimizations, which consistently resulted in a good inferred model with an average error of 0.074 ± 0.001 *SD*. The model with the lowest error (0.072) among the five runs is reported, and Table 1 shows the values of all the parameters in the model.

3.3 | Parameter estimation experiments

3.3.1 | Dynamics of wild-type strain growth in glucose or cellobiose

The mathematical model with the inferred parameters was able to recapitulate the growth dynamics and metabolic consumptions of wild-type *C. japonicus* grown in either glucose or cellobiose (Figure 3), which resulted in very similar growth rates of 0.4 h^{-1} for the experimental and simulated data (Table 2). Figure 3a shows the in vivo and in silico dynamics of cell biomass and metabolic consumption in the wild-type strain growing in glucose media. The model recapitulated the lag, exponential, and stationary phases of the cell biomass concentration (red line) together with the dynamic extracellular concentration of glucose (purple line), with an R^2 of 0.978 (Table 3). Figure 3b shows how the same model and parameters also recapitulated the cell biomass concentration and metabolic consumption dynamics of the wild-type strain in cellobiose media, including the experimentally observed extracellular degradation of cellobiose (yellow line) into glucose (purple line), with an R^2 of 0.979 (Table 3).

3.3.2 | Dynamics of β-glucosidase knockout strains growth in glucose or cellobiose

Next, we performed growth experiments and model simulations in single and double β-glucosidase knockout mutants of *C. japonicus* grown in either glucose or cellobiose (Figure 4). The model and parameters were the same as in the wild-type strain simulations except for the knockout enzymes, which concentrations and rates were set to zero to simulate enzyme gene deletions. Figure 4 shows the in vivo and in silico dynamics in single and double *C. japonicus* mutants grown in glucose or cellobiose media. The results demonstrate that the knockouts of the β-glucosidases *cel*3A or/and *cel*3B had no effect on the bacterial growth dynamics in glucose media in terms of cell biomass and metabolite consumption, a behavior that the model recapitulated with an R^2 of 0.99 for the three experiments (Table 3). Indeed, the three mutant strains produced a similar growth rate as the wild-type strain (0.4 h^{-1}; Table 2). When grown in

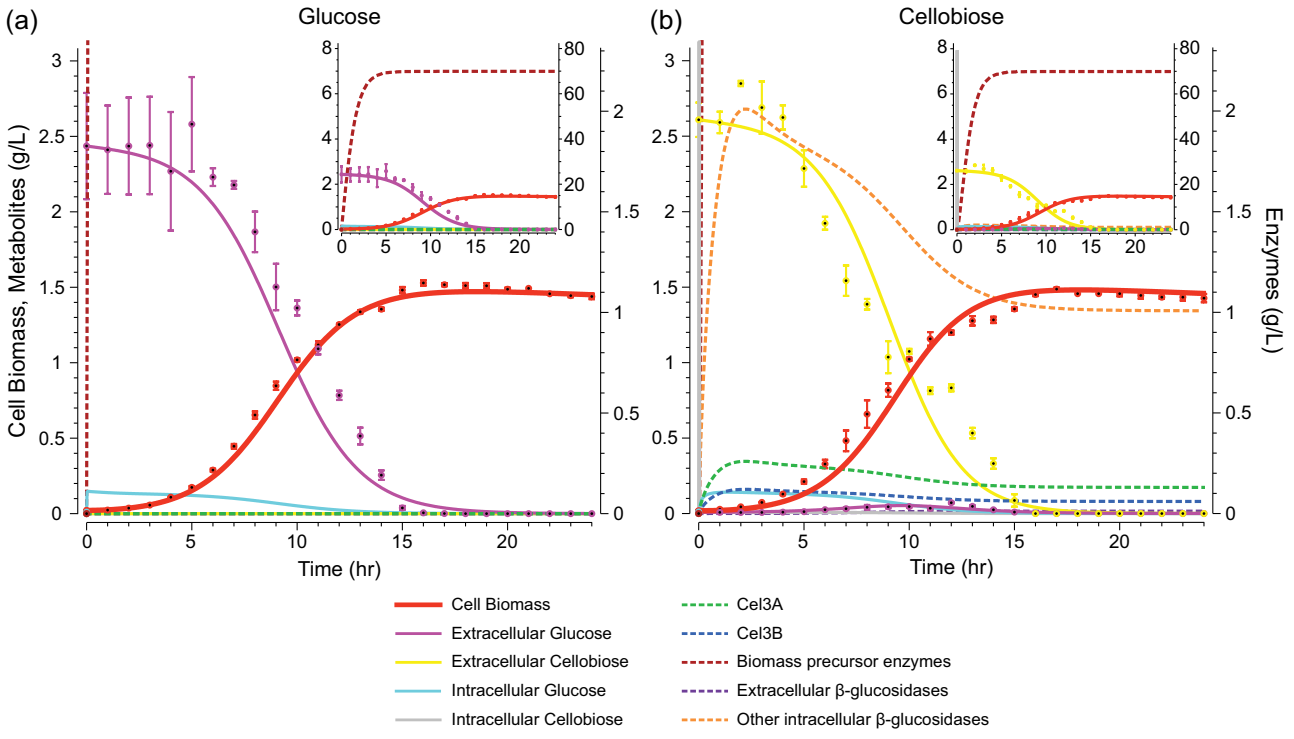

FIGURE 3 Experimental and inferred model dynamics of wild-type *Cellvibriojaponicus* growth, metabolite consumption, and β-glucosidase expressions in glucose or cellobiose media. The model simulation (solid lines for cell biomass and metabolites concentration; dashed lines for enzyme concentrations) recapitulates the bacterial growth dynamics and extracellular concentrations of glucose and cellobiose metabolites from the in vivo experiments (dots) using either 0.25% (wt/vol) glucose (a) or 0.25% (wt/vol) cellobiose (b) as the sole carbon source. Inset graphs show a zoom-out of concentration profiles. Error bars indicate standard deviation calculated from biological triplicate experiments [Color figure can be viewed at wileyonlinelibrary.com]

TABLE 2 Growth rates of in vivo (average) and in silico experiments

Medium	Strain	In vivo growth rate (h^{-1})	In silico growth rate (h^{-1})
0.25% Glucose	Wild type	0.411	0.386
0.25% Glucose	Δ*cel3A*	0.424	0.396
0.25% Glucose	Δ*cel3B*	0.410	0.384
0.25% Glucose	Δ*cel3A* Δ*cel3B*	0.411	0.396
0.25% Cellobiose	Wild type	0.409	0.403
0.25% Cellobiose	Δ*cel3A*	0.414	0.396
0.25% Cellobiose	Δ*cel3B*	0.361	0.331
0.25% Cellobiose	Δ*cel3A* Δ*cel3B*	0.267	0.219
0.125% Glucose/0.125% Cellobiose	Wild type	0.416	0.405
0.125% Glucose/0.125% Cellobiose	Δ*cel3A*	–	0.381
0.125% Glucose/0.125% Cellobiose	Δ*cel3B*	–	0.337
0.125% Glucose/0.125% Cellobiose	Δ*cel3A* Δ*cel3B*	–	0.238

cellobiose media, the Δcel3A strain resulted in the same growth ($0.4\ h^{-1}$) and metabolite consumption dynamics as in the wild-type as recapitulated by the model with an R^2 of 0.985 (Figure 4b). In contrast, the Δ*cel3B* strain resulted in slower growth dynamics in cellobiose media ($0.36\ h^{-1}$), a behavior that the model also recapitulated with an R^2 of 0.976 and a reduced growth rate of $0.33\ h^{-1}$ (Figure 4d). Interestingly, the double knockout Δ*cel3A* Δ*cel3B* strain in cellobiose media resulted in the slowest growth dynamics ($0.27\ h^{-1}$), as the model also recapitulated with an R^2 of 0.996 and growth rate of $0.22\ h^{-1}$ (Figure 4f).

The mechanistic model can explain the different growth dynamics of the mutants in terms of the higher expression of the different β-glucosidases, which compensate for the effects of the gene knockouts. Comparing the enzyme concentrations during growth in cellobiose in the mutant Δ*cel3A* strain (Figure 4b) with those in the wild-type (Figure 3b), the model showed no significant difference in the concentration of Cel3B (dashed blue line) or other intracellular β-glucosidases (dashed orange line) due to the experimentally derived high catalytic efficiency of Cel3B. In contrast, in the Δ*cel3B* strain growing in cellobiose (Figure 4d) the model showed an increased concentration in both Cel3A (dashed green line) and other β-glucosidases (dashed orange line) to be necessary to compensate for the loss of Cel3B. In the Δ*cel3A* Δ*cel3B* double mutant grown in cellobiose (Figure 4f), the model showed a very large increase in concentration of other β-glucosidases (dashed orange line) with respect the wild-type, a behavior that was not enough to maintain a high growth rate due to the predicted low efficiency of these β-glucosidases. In addition, the model predicted an accumulation of extracellular glucose (purple solid line) proportional to the reduction of growth rates in the mutant strains with cellobiose media due to the cumulative activity of extracellular β-glucosidases, which concentration was the highest in the Δ*cel3A* Δ*cel3B* double mutant (Figure 4f).

TABLE 3 Coefficients of determination comparing the dynamics of cell biomass and extracellular metabolic concentrations between in vivo (average) and in silico experiments

Medium	Strain	Coefficient of determination (R^2)
0.25% Glucose	Wild type	0.978
0.25% Glucose	Δ*cel3A*	0.994
0.25% Glucose	Δ*cel3B*	0.997
0.25% Glucose	Δ*cel3A* Δ*cel3B*	0.997
0.25% Cellobiose	Wild type	0.979
0.25% Cellobiose	Δ*cel3A*	0.985
0.25% Cellobiose	Δ*cel3B*	0.976
0.25% Cellobiose	Δ*cel3A* Δ*cel3B*	0.996
0.125% Glucose/ 0.125% Cellobiose	Wild type	0.938

3.4 | Predictive experiments

3.4.1 | Dynamics of wild-type growth in glucose and cellobiose mixed media

To test the predictive power of the model with the inferred parameters, a novel experiment with glucose and cellobiose mixed media not included in the training data set was performed experimentally and simulated with the model. Figure 5 shows the in vivo experimental and corresponding model predicted growth dynamics in mixed media of 0.125% glucose and 0.125% cellobiose for the wild-type strain of *C. japonicus*. The results showed non-diauxic concurrent utilization of both glucose and cellobiose carbon sources resulting in a single exponential growth phase, a behavior that the

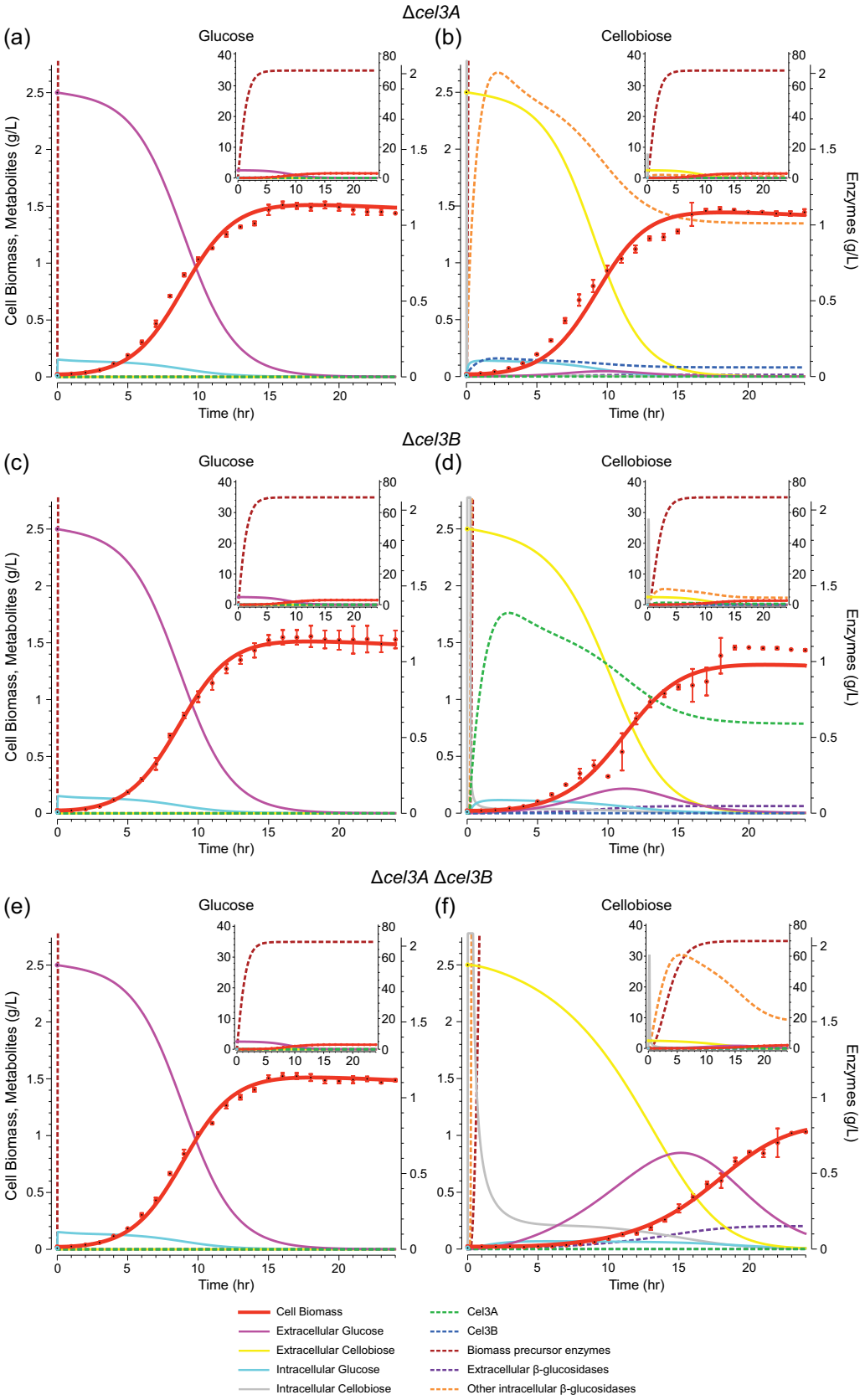

FIGURE 4 (Continued)

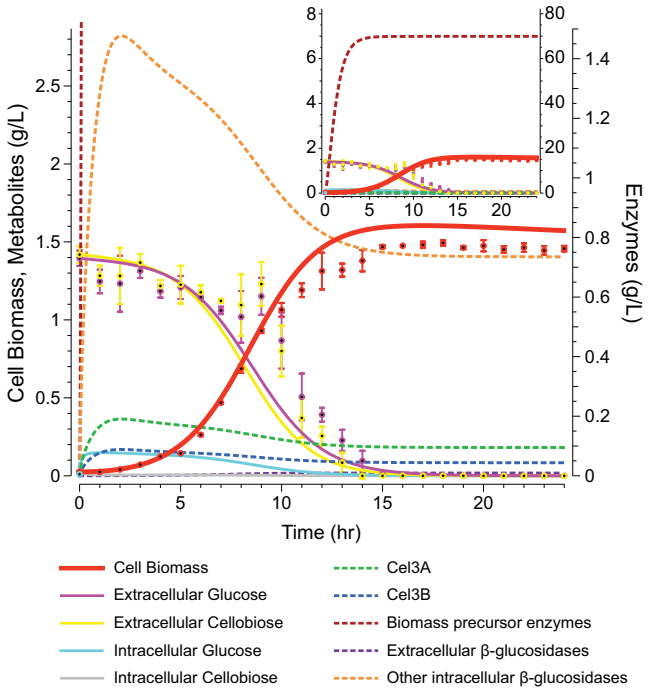

FIGURE 5 Model prediction and experimental validation of non-diauxic growth, metabolite consumption, and β-glucosidase expressions in mixed glucose and cellobiose media. The model simulations (solid lines for cell biomass and metabolites concentration; dashed lines for enzyme concentrations) predict the non-diauxic growth dynamics of wild-type *Cellvibriojaponicus* in a mixed media containing both 0.125% (wt/vol) glucose and 0.125% (wt/vol) cellobiose as carbon sources. The predicted cell biomass and metabolite dynamics were validated in vivo (dots). Inset graphs show a zoom-out of concentration profiles. Error bars indicate standard deviation from biological triplicate experiments [Color figure can be viewed at wileyonlinelibrary.com]

model correctly predicted with an R^2 of 0.938 (Table 3). Remarkably, the model predicted a growth rate in the mixed media (0.405 h^{-1}) that closely mirrored the growth rate observed experimentally (0.416 h^{-1}). Furthermore, the model predicted glucose concentration levels to be slightly higher than cellobiose levels in the media during the exponential growth phase, a phenomenon that was experimentally observed as well. Finally, the model predicted a slight decrease in the concentration levels of β-glucosidase enzymes in the mixed media (Figure 5, dashed lines) with respect to the single cellobiose carbon source (Figure 3B, dashed lines) due to the decreased concentration levels of extracellular cellobiose in the mixed media.

3.4.2 | Dynamics of β-glucosidase knockout strains growth in glucose and cellobiose mixed media

Next, we used the model to predict the growth dynamics of *C. japonicus* single and double β-glucosidase mutant strains in glucose and cellobiose mixed media conditions. Figure 6 shows the predicted dynamics in the single and double mutants of Δ*cel3A* and Δ*cel3B*, resulting in similar decreases in growth rates as the same mutants growing in cellobiose as a single substrate (Table 2). Interestingly, the model predicted a substantial increase in the concentrations of glucose in the media with respect to cellobiose in the Δ*cel3B* strain (Figure 6b) due to the combined effect of slower growth dynamics and unaffected extracellular cellobiose degradation. This phenomenon was not observed in the Δ*cel3A* strain (Figure 6a), which exhibits the same dynamics as the wild-type strain growing in mixed media (Figure 5), but was exacerbated in the Δ*cel3A* Δ*cel3B* double mutant (Figure 6c), since the growth rate was slower than in the single mutants. Similar to the growth of the Δ*cel3A* and Δ*cel3B* single gene deletion strains in cellobiose-only media (Figure 4), the knockout of *cel3A* did not result in a significant increase in the concentration of the enzymes (Figure 6A, dashed lines), but a knockout of the *cel3B* gene resulted in higher concentration levels of Cel3A and other intracellular β-glucosidases (Figure 6B, green and orange dashed lines, respectively). The concentrations of other intracellular β-glucosidases reached the highest value in mixed media growth for the Δ*cel3A* Δ*cel3B* double mutant strain (Figure 6C, orange dashed line), although this concentration was lower than during the growth in cellobiose-only media (Figure 4f).

3.5 | Design strategies for maximizing cellobiose-specific degradation rate

The proposed kinetic model can be employed to design strategies for industrially relevant genetic strains of *C. japonicus*. In particular, maximizing the cellobiose-specific degradation rate represents an optimization strategy towards the efficient production of value-added metabolites derived from lignocellulose, such as ethanol or succinate. Towards this, the model can predict the cellobiose-specific degradation rate under any combination of deletion and overexpression of the relevant enzymes. We simulated all combinations of one and two genetic perturbations, including deletions and medium and high overexpression, for all β-glucosidase genes in the model. Figure 7 shows the specific degradation rate of cellobiose

FIGURE 4 Experimental and inferred model dynamics for cell growth, metabolite consumption, and β-glucosidase expressions of deletion mutants grown with either glucose or cellobiose media. The model simulations (solid lines for cell biomass and metabolites concentration; dashed lines for enzyme concentrations) recapitulates the experimental *Cellvibriojaponicus* growth dynamics (dots) in single and double mutants in media containing either cellobiose or glucose as the sole carbon sources. (a,b) Growth dynamics of a Δ*cel3A* mutant in 0.25% (wt/vol) glucose (a) or 0.25% (wt/vol) cellobiose (b). (c,d) Growth dynamics of a Δ*cel3B* mutant in glucose (c) or cellobiose (d). (e,f) Growth dynamics of a Δ*cel3A* Δ*cel3B* double mutant in glucose (e) or cellobiose (f). Inset graphs show a zoom-out of concentration profiles. Error bars indicate standard deviation from biological triplicate experiments [Color figure can be viewed at wileyonlinelibrary.com]

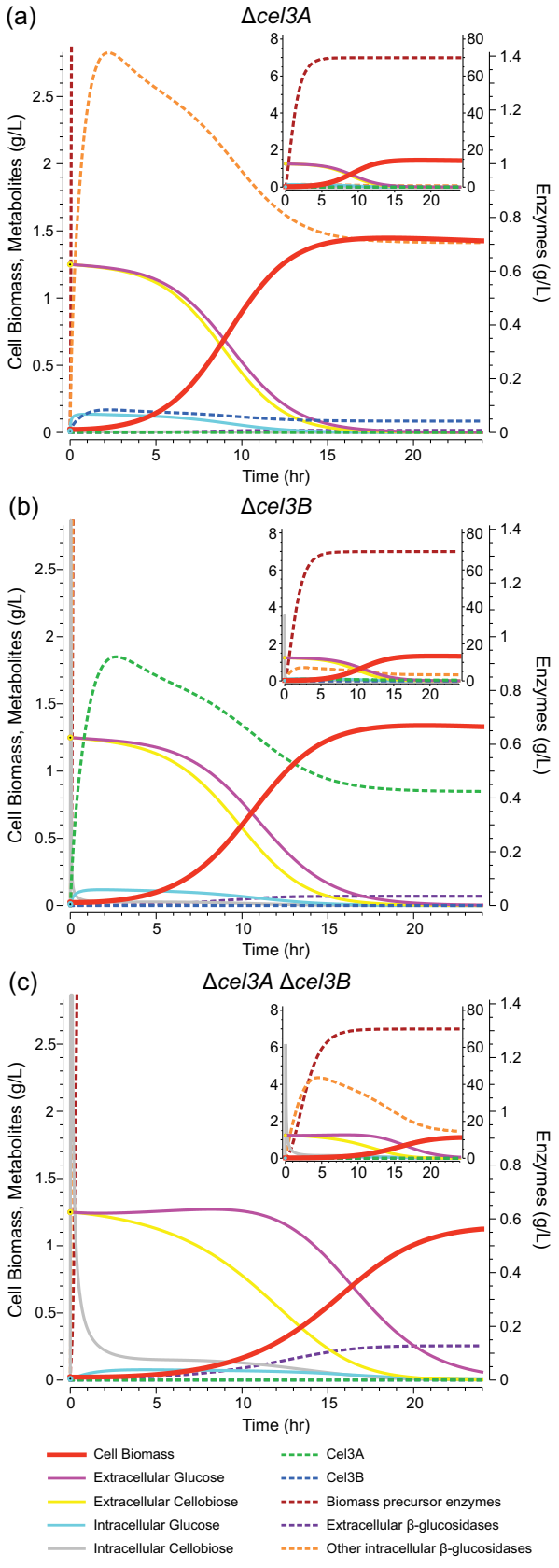

obtained for each of the perturbation combination simulations, together with the baseline rate obtained in the wild-type strain. The results show that Cel3B and the extracellular β-glucosidases have the highest impact on the cellobiose-specific degradation rate. In particular, the best-predicted strategy for maximizing the cellobiose-specific degradation rate is the deletion of the *cel3B* gene together with a high overexpression of the extracellular β-glucosidases genes. This mutant strain is predicted to result in a 3.8-fold increase in cellobiose-specific degradation rate with respect to the wild-type strain. Future work will engineer these strains in vivo towards the validation of these results and the study of their feasibility for specific bioengineering applications.

4 | DISCUSSION

We presented here a combined in vivo and in silico approach for developing a *Cellvibrio japonicus* kinetic model that mechanistically accounts for (i) bacterial growth dynamics, (ii) metabolite consumption, and (iii) genetic knockouts of key enzymes. The proposed model consisted of a set of ODEs utilizing Michaelis–Menten kinetics for the metabolic reactions in addition to specific terms for the uptake of metabolites into the cell, expression, secretion, and dilution of different β-glucosidase enzymes, and cell biomass growth. The kinetic parameters of the known β-glucosidases were derived from in vitro enzymatic experiments. To infer the unknown parameters, we developed a computational methodology based on genetic algorithms that takes as input the growth dynamics and metabolic concentrations from in vivo experiments with both wild-type and mutant strains to infer a parameter set able to recapitulate the bacterial growth dynamics and metabolic consumptions during the lag, exponential, and stationary phases under multiple substrates and genetic backgrounds.

The model with the single set of inferred parameters could account for the dynamics of cellobiose degradation and glucose

FIGURE 6 Model predictions of growth, metabolic consumption, and β-glucosidase expression for gene deletion strains in mixed glucose and cellobiose media. The model simulation (solid lines for cell biomass and metabolites concentration; dashed lines for enzyme concentrations) predicts the growth dynamics for mutant *Cellvibrio japonicus* strains in media containing both 0.125% (wt/vol) glucose and 0.125% (wt/vol) cellobiose. (a) Growth dynamics of a Δ*cel3A* mutant in mixed glucose and cellobiose media. (b) Growth dynamics of a Δ*cel3B* mutant in mixed glucose and cellobiose media. (c) Growth dynamics of a Δ*cel3A* Δ*cel3B* double mutant in mixed glucose and cellobiose media. Inset graphs show a zoom-out of concentration profiles [Color figure can be viewed at wileyonlinelibrary.com]

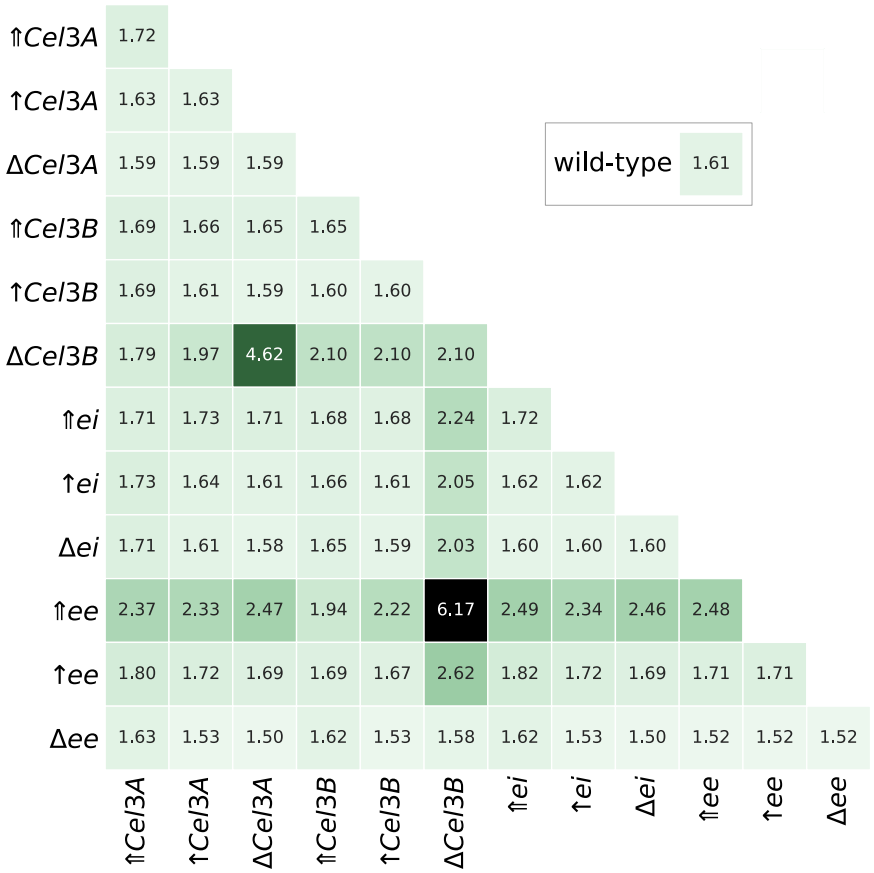

FIGURE 7 Model predictions of cellobiose-specific degradation rates for β-glucosidase gene deletions and overexpressions. Model simulations of *Cellvibrio japonicus* growth in 0.25% (wt/vol) cellobiose media with single and double β-glucosidase gene perturbations, including knock-out (Δ), medium (↑), or high (⇑) overexpression levels, predict the specific degradation rates of cellobiose (g cellobiose/(g cell biomass • h)). Gene perturbations are simulated by multiplying the specific rates of *Cel3A*, *Cel3B*, other internal β-glucosidases, and the secreted β-glucosidases (β_{Cel3A}, β_{Cel3B}, β_{ei}, and β_{ee}, respectively) by zero (knock-out), 2 (medium overexpression), and 10 (high overexpression). The specific degradation rate of cellobiose in the wild-type strain simulation is shown for comparison [Color figure can be viewed at wileyonlinelibrary.com]

utilization experimentally obtained in wild-type and gene-knockout mutants of *C. japonicus*. The inferred model recapitulated all the experimental dynamics in terms of cell biomass and metabolite concentrations for all the experiments in the training data set. In addition, the model simulation showed how the concentration levels of the β-glucosidases are modulated during the knockouts. In the case of Cel3A, despite a low catalytic efficiency for cellobiose (as obtained in vitro), it had an increased concentration in a Δ*cel3B* strain, which accounts for the minimal decrease in cell growth rate. In contrast, Cel3B has a high catalytic efficiency for cellobiose and therefore its concentration was not increased in a Δ*cel3A* strain. The Δ*cel3A* Δ*cel3B* double mutant displayed a very high increase in other intracellular β-glucosidase concentration, but due to their predicted low catalytic efficiency the cell growth rate was still severely reduced. Future work will generate and analyze metabolite and proteomics data from the mutant strains to further validate the model predicted dynamics for enzyme secretions and nutrient concentrations.

The predictive power of the inferred model was tested with a growth experiment of the wild-type strain with mixed glucose and cellobiose media. The model predicted non-diauxic growth with a simultaneous consumption of both carbon sources, which was indeed validated in vivo. In addition, further predictions were presented for the growth in mixed glucose and cellobiose media for the β-glucosidase mutant strains. Our results indicated a decreased growth rate similar to the cellobiose media growth dynamics and a decreased cellobiose concentration with respect to glucose for the Δ*cel3A* Δ*cel3B* double mutant. Finally, a design strategy to maximize the specific degradation rate of cellobiose in *C. japonicus* was derived from the model. The analysis predicted that a mutant strain with a deletion of the *cel3B* gene together with a high overexpression of the extracellular β-glucosidases genes resulted in a substantial increase in cellobiose-specific degradation rate with respect the wild-type strain. These analyses show the capacity of the proposed model to guide the design of industrially relevant optimizations that would be essential for the production of value-added metabolites derived from lignocellulose.

5 | CONCLUSION

The presented methodology can provide insights into the kinetic relationships of different enzymes during the degradation of carbohydrates in microorganisms, and further modeling extensions and pathway analysis tools can include detailed information regarding the regulatory dynamics of the essential enzymes (Hari & Lobo, 2020; Koutinas et al., 2011; Tsipa, Koutinas, Usaku, & Mantalaris, 2018). The study of cellulose degradation and associated enzymes could have significant implications in the development of efficient cellulose bioconversion into renewable fuels and chemicals (Martien & Amador-Noguez, 2017). *C. japonicus* shows incredible

potential as a model organism for research with its ability to completely degrade lignocellulose and other polymeric materials. The methodology and model presented in this study is the first step towards developing a comprehensive metabolic and regulatory network for the degradation of lignocellulose in *C. japonicus*, paving the way for the comprehensive understanding of polysaccharide utilization dynamics by microorganisms.

ACKNOWLEDGMENTS

We thank Julia Wolf for assistance with experiments, Jackson Narrett for the electron microscopy image of *C. japonicus* in the graphical abstract, and the members of the Lobo and Gardner research groups for helpful discussions. Research performed in the Gardner lab was supported by the U.S. Department of Energy, Office of Science, Office of Biological and Environmental Research, under award DE-SC0014183. Computations used the UMBC High Performance Computing Facility (HPCF) supported by the NSF grants OAC-1726023, CNS-0821258, CNS-1228778, and DMS-0821311. This report was prepared as an account of work sponsored by an agency of the U.S. Government. Neither the U.S. Government nor any agency thereof, nor any of their employees, makes any warranty, expressed or implied, or assumes any legal liability or responsibility for the accuracy, completeness, or usefulness of any information, apparatus, product, or process disclosed, or represents that its use would not infringe privately owned rights. Reference herein to any specific commercial product, process, or service by trade name, trademark, manufacturer, or otherwise does not necessarily constitute or imply its endorsement, recommendation, or favoring by the U.S. Government or any agency thereof. The views and opinions of the authors expressed herein do not necessarily state or reflect those of the U.S. Government or any agency thereof.

CONFLICT OF INTERESTS

The authors declare that there are no conflict of interests.

AUTHOR CONTRIBUTIONS

Jeanice Hwang, Archana Hari, and Daniel Lobo constructed the mathematical model. Jeanice Hwang and Daniel Lobo developed the simulator and optimization algorithms and generated and analyzed the model results. Raymond Cheng performed *C. japonicus* growth analysis experiments and metabolite quantification and analysis. Jeffrey G. Gardner and Daniel Lobo conceived the study, provided overall direction, and secured funding. Jeanice Hwang and Daniel Lobo wrote the manuscript draft and all authors edited and approved the final manuscript.

ORCID

Daniel Lobo http://orcid.org/0000-0003-4666-6118

REFERENCES

Chassagnole, C., Noisommit-Rizzi, N., Schmid, J. W., Mauch, K., & Reuss, M. (2002). Dynamic modeling of the central carbon metabolism of *Escherichia coli*. *Biotechnology and Bioengineering*, *79*(1), 53–73. https://doi.org/10.1002/bit.10288

DeBoy, R. T., Mongodin, E. F., Fouts, D. E., Tailford, L. E., Khouri, H., Emerson, J. B., … Nelson, K. E. (2008). Insights into plant cell wall degradation from the genome sequence of the soil bacterium Cellvibrio japonicus. *Journal of Bacteriology*, *190*(15), 5455–5463. https://doi.org/10.1128/JB.01701-07

Fox, J. M., Levine, S. E., Blanch, H. W., & Clark, D. S. (2012). An evaluation of cellulose saccharification and fermentation with an engineered *Saccharomyces cerevisiae* capable of cellobiose and xylose utilization. *Biotechnology Journal*, *7*(3), 361–373. https://doi.org/10.1002/biot.201100209

Gardner, J. G., Crouch, L., Labourel, A., Forsberg, Z., Bukhman, Y. V., Vaaje-Kolstad, G., … Keating, D. H. (2014). Systems biology defines the biological significance of redox-active proteins during cellulose degradation in an aerobic bacterium. *Molecular Microbiology*, *94*(5), 1121–1133. https://doi.org/10.1111/mmi.12821

Gardner, J. G., & Keating, D. H. (2010). Requirement of the type II secretion system for utilization of cellulosic substrates by *Cellvibrio japonicus*. *Applied and Environmental Microbiology*, *76*(15), 5079–5087. https://doi.org/10.1128/AEM.00454-10

Gomez-Flores, M., Nakhla, G., & Hafez, H. (2015). Microbial kinetics of *Clostridium termitidis* on cellobiose and glucose for biohydrogen production. *Biotechnology Letters*, *37*(10), 1965–1971. https://doi.org/10.1007/s10529-015-1891-4

Gomez-Flores, M., Nakhla, G., & Hafez, H. (2017). Hydrogen production and microbial kinetics of *Clostridium termitidis* in mono-culture and co-culture with *Clostridium beijerinckii* on cellulose. *AMB Express*, *7*(1), 84. https://doi.org/10.1186/s13568-016-0256-2

Goswami, S., Gupta, N., & Datta, S. (2016). Using the B-glucosidase catalyzed reaction product glucose to improve the ionic liquid tolerance of B-glucosidases. *Biotechnology for Biofuels*, *9*(1), 1–12. https://doi.org/10.1186/s13068-016-0484-3

Hall, B. G., Acar, H., Nandipati, A., & Barlow, M. (2014). Growth rates made easy. *Molecular Biology and Evolution*, *31*(1), 232–238. https://doi.org/10.1093/molbev/mst187

Hari, A., & Lobo, D. (2020). Fluxer: A web application to compute, analyze and visualize genome-scale metabolic flux networks. *Nucleic Acids Research*, *48*(W1), W427–W435. https://doi.org/10.1093/nar/gkaa409

Jahan, N., Maeda, K., Matsuoka, Y., Sugimoto, Y., & Kurata, H. (2016). Development of an accurate kinetic model for the central carbon metabolism of *Escherichia coli*. *Microbial Cell Factories*, *15*(1), 1–19. https://doi.org/10.1186/s12934-016-0511-x

Jeoh, T., Cardona, M. J., Karuna, N., Mudinoor, A. R., & Nill, J. (2017). Mechanistic kinetic models of enzymatic cellulose hydrolysis—A review. *Biotechnology and Bioengineering*, *114*(7), 1369–1385. https://doi.org/10.1002/bit.26277

Kadam, K. L., Rydholm, E. C., & McMillan, J. D. (2004). Development and validation of a kinetic model for enzymatic saccharification of lignocellulosic biomass. *Biotechnology Progress*, *20*, 698–705. https://doi.org/10.1021/bp034316x

Kadir, T. A. A., Mannan, A. A., Kierzek, A. M., McFadden, J., & Shimizu, K. (2010). Modeling and simulation of the main metabolism in *Escherichia coli* and its several single-gene knockout mutants with experimental verification. *Microbial Cell Factories*, *9*, 1–21. https://doi.org/10.1186/1475-2859-9-88

Koutinas, M., Kiparissides, A., Silva-Rocha, R., Lam, M. C., Martins dos Santos, V. A. P., de Lorenzo, V., … Mantalaris, A. (2011). Linking genes to microbial growth kinetics—An integrated biochemical systems engineering approach. *Metabolic Engineering*, *13*(4), 401–413. https://doi.org/10.1016/j.ymben.2011.02.001

Kurata, H., & Sugimoto, Y. (2018). Improved kinetic model of *Escherichia coli* central carbon metabolism in batch and continuous cultures. *Journal of Bioscience and Bioengineering*, *125*(2), 251–257. https://doi.org/10.1016/j.jbiosc.2017.09.005

Kuusk, S., Sørlie, M., & Väljamäe, P. (2015). The predominant molecular state of bound enzyme determines the strength and type of product inhibition in the hydrolysis of recalcitrant polysaccharides by processive enzymes. *Journal of Biological Chemistry*, *290*(18), 11678–11691. https://doi.org/10.1074/jbc.M114.635631

Kwon, Y., & Engler, C. (2005). Kinetic models for growth and product formation on multiple substrates. *Biotechnology and Bioprocess Engineering*, *10*(1), 587–592. https://doi.org/10.1007/BF02932299

Lobikin, M., Lobo, D., Blackiston, D. J., Martyniuk, C. J., Tkachenko, E., & Levin, M. (2015). Serotonergic regulation of melanocyte conversion: A bioelectrically regulated network for stochastic all-or-none hyperpigmentation. *Science Signaling*, *8*(397), ra99. https://doi.org/10.1126/scisignal.aac6609

Lobo, D., & Levin, M. (2015). Inferring regulatory networks from experimental morphological phenotypes: A computational method reverse-engineers planarian regeneration. *PLoS Computational Biology*, *11*, e1004295. https://doi.org/10.1371/journal.pcbi.1004295

Lobo, D., & Vico, F. J. (2010a). Evolution of form and function in a model of differentiated multicellular organisms with gene regulatory networks. *Biosystems*, *102*, 112–123. https://doi.org/10.1016/j.biosystems.2010.08.003

Lobo, D., & Vico, F. J. (2010b). Evolutionary development of tensegrity structures. *Biosystems*, *101*, 167–176. https://doi.org/10.1016/j.biosystems.2010.06.005

López-Pérez, P. A., Puebla, H., Velázquez Sánchez, H. I., & Aguilar-López, R. (2016). Comparison tools for parametric identification of kinetic model for ethanol production using evolutionary optimization approach. *International Journal of Chemical Reactor Engineering*, *14*(6), 1201–1209. https://doi.org/10.1515/ijcre-2016-0045

Mahfoud, S. W. (1992). Crowding and preselection revisited. In R. Manner, & B. Manderick (Eds.), *Parallel problem solving from nature* (Vol. 2, pp. 27–36). Amsterdam: Elsevier.

Martien, J. I., & Amador-Noguez, D. (2017). Recent applications of metabolomics to advance microbial biofuel production. *Current Opinion in Biotechnology*, *43*, 118–126. https://doi.org/10.1016/j.copbio.2016.11.006

Mehmood, M. A., Shahid, I., Hussain, K., Latif, F., & Rajoka, M. I. (2014). Thermodynamic properties of the β-glucosidase from *Thermotoga maritima* extend the upper limit of thermophilicity. *Protein and Peptide Letters*, *21*(12), 1282–1288.

Meng, D. D., Ying, Y., Zhang, K.D.i, Lu, M., & Li, F. L. (2015). Depiction of carbohydrate-active enzyme diversity in *Caldicellulosiruptor* sp. F32 at the genome level reveals insights into distinct polysaccharide degradation features. *Molecular BioSystems*, *11*(11), 3164–3173. https://doi.org/10.1039/c5mb00409h

Millard, P., Smallbone, K., & Mendes, P. (2017). Metabolic regulation is sufficient for global and robust coordination of glucose uptake, catabolism, energy production and growth in *Escherichia coli*. *PLOS Computational Biology*, *13*(2), e1005396. https://doi.org/10.1371/journal.pcbi.1005396

Moldes, A. B., Alonso, J. L., & Parajó, J. C. (1999). Cogeneration of cellobiose and glucose from pretreated wood and bioconversion to lactic acid: A kinetic study. *Journal of Bioscience and Bioengineering*, *87*(6), 787–792. https://doi.org/10.1016/S1389-1723(99)80154-6

Mutturi, S., & Lidén, G. (2014). Model-based estimation of optimal temperature profile during simultaneous saccharification and fermentation of *Arundo donax*. *Biotechnology and Bioengineering*, *111*(5), 866–875. https://doi.org/10.1002/bit.25165

Nelson, C. E., Attia, M. A., Rogowski, A., Morland, C., Brumer, H., & Gardner, J. G. (2017). Comprehensive functional characterization of the glycoside hydrolase family 3 enzymes from Cellvibrio japonicus reveals unique metabolic roles in biomass saccharification. *Environmental Microbiology*, *19*(12), 5025–5039. https://doi.org/10.1111/1462–2920.13959

Nelson, C. E., & Gardner, J. G. (2015). In-frame deletions allow functional characterization of complex cellulose degradation phenotypes in *Cellvibrio japonicus*. *Applied and Environmental Microbiology*, *81*(17), AEM.00847-15. https://doi.org/10.1128/AEM.00847-15

Nelson, C. E., Rogowski, A., Morland, C., Wilhide, J. A., Gilbert, H. J., & Gardner, J. G. (2017). Systems analysis in Cellvibrio japonicus resolves predicted redundancy of β-glucosidases and determines essential physiological functions. *Molecular Microbiology*, *104*(2), 294–305. https://doi.org/10.1111/mmi.13625

Neto, J. M., Dos Reis Garcia, D., Rueda, S. M. G., & Da Costa, A. C. (2013). Study of kinetic parameters in a mechanistic model for enzymatic hydrolysis of sugarcane bagasse subjected to different pretreatments. *Bioprocess and Biosystems Engineering*, *36*(11), 1579–1590. https://doi.org/10.1007/s00449-013-0930-6

Oh, K. K., Kim, S. W., Jeong, Y. S., & Hong, S. I. (2000). Bioconversion of cellulose into ethanol by nonisothermal simultaneous saccharification and fermentation. *Applied Biochemistry and Biotechnology - Part A Enzyme Engineering and Biotechnology*, *89*(1), 15–30. https://doi.org/10.1385/ABAB:89:1:15

Park, J., Lang, J., Thamaraiselvi, K., Kukor, J. J., & Abriola, L. M. (2008). Induction kinetics of aerobic toluene degradation as a function of carbon starvation history. *Process Biochemistry*, *43*(12), 1345–1351. https://doi.org/10.1016/j.procbio.2008.08.004

Petzold, L. (1983). Automatic selection of methods for solving stiff and nonstiff systems of ordinary differential equations. *SIAM Journal on Scientific and Statistical Computing*, *4*(1), 136–148. https://doi.org/10.1137/0904010

Philippidis, G. P., & Hatzis, C. (1997). Biochemical engineering analysis of critical process factors in the biomass-to-ethanol technology. *Biotechnology Progress*, *13*(3), 222–231. https://doi.org/10.1021/bp970017u

Riemann, L., & Azam, F. (2002). Widespread N-acetyl-D-glucosamine uptake among pelagic marine bacteria and its ecological implications. *Applied and Environmental Microbiology*, *68*(11), 5554–5562. https://doi.org/10.1128/AEM.68.11.5554–5562.2002

Rojo, F. (2010). Carbon catabolite repression in Pseudomonas: Optimizing metabolic versatility and interactions with the environment. *FEMS Microbiology Reviews*, *34*(5), 658–684. https://doi.org/10.1111/j.1574–6976.2010.00218.x

Sakimoto, K., Kanna, M., & Matsumura, Y. (2017). Kinetic model of cellulose degradation using simultaneous saccharification and fermentation. *Biomass and Bioenergy*, *99*, 116–121. https://doi.org/10.1016/j.biombioe.2017.02.016

Shadbahr, J., Khan, F., & Zhang, Y. (2017). Kinetic modeling and dynamic analysis of simultaneous saccharification and fermentation of cellulose to bioethanol. *Energy Conversion and Management*, *141*, 236–243. https://doi.org/10.1016/j.enconman.2016.08.025

Shadbahr, J., Zhang, Y., Khan, F., & Hawboldt, K. (2018). Multi-objective optimization of simultaneous saccharification and fermentation for cellulosic ethanol production. *Renewable Energy*, *125*, 100–107. https://doi.org/10.1016/j.renene.2018.02.106

Shen, J., & Agblevor, F. A. (2010). The operable modeling of simultaneous saccharification and fermentation of ethanol production from cellulose. *Applied Biochemistry and Biotechnology*, *160*(3), 665–681. https://doi.org/10.1007/s12010-009-8650-8

Shin, D., Yoo, A., Kim, S. W., & Yang, D. R. (2006). Cybernetic modeling of simultaneous saccharification and fermentation for ethanol production from steam-exploded wood with Brettanomyces custersii. *Journal of Microbiology and Biotechnology*, *16*(9), 1355–1361.

Smallbone, K., Messiha, H. L., Carroll, K. M., Winder, C. L., Malys, N., Dunn, W. B., … Mendes, P. (2013). A model of yeast glycolysis based on a consistent kinetic characterisation of all its enzymes. *FEBS Letters*, *587*(17), 2832–2841. https://doi.org/10.1016/j.febslet.2013.06.043

Steuer, R., Gross, T., Selbig, J., & Blasius, B. (2006). Structural kinetic modeling of metabolic networks. *Proceedings of the National Academy*

of Sciences, *103*(32), 11868–11873. https://doi.org/10.1073/pnas.0600013103

Tsipa, A., Koutinas, M., Usaku, C., & Mantalaris, A. (2018). Optimal bioprocess design through a gene regulatory network—Growth kinetic hybrid model: Towards replacing monod kinetics. *Metabolic Engineering*, *48*(March), 129–137. https://doi.org/10.1016/j.ymben.2018.04.023

Whitley, D., Rana, S., & Heckendorn, R. B. (1999). The island model genetic algorithm: On separability, population size and convergence. *Journal of Computing and Information Technology*, *7*, 33–48.

Wu, J., Du, G., Chen, J., & Zhou, J. (2015). Enhancing flavonoid production by systematically tuning the central metabolic pathways based on a CRISPR interference system in *Escherichia coli*. *Scientific Reports*, *5*(May), 1–14. https://doi.org/10.1038/srep13477

How to cite this article: Hwang J, Hari A, Cheng R, Gardner JG, Lobo D. Kinetic modeling of microbial growth, enzyme activity, and gene deletions: An integrated model of β-glucosidase function in *Cellvibrio japonicus*. *Biotechnology and Bioengineering*. 2020;1–15. https://doi.org/10.1002/bit.27544